

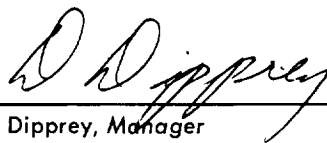
NATIONAL AERONAUTICS AND SPACE ADMINISTRATION

Technical Report No. 32-788

*Experimental Measurements on a Rotating
Detonation-Like Wave Observed During
Liquid Rocket Resonant Combustion*

R. M. Clayton

R. S. Rogero

A handwritten signature in cursive script, reading "D. Dipprey", is written over a horizontal line.

D. Dipprey, Manager
Liquid Propulsion Section

JET PROPULSION LABORATORY
CALIFORNIA INSTITUTE OF TECHNOLOGY
PASADENA, CALIFORNIA

August 15, 1965

Copyright © 1965
Jet Propulsion Laboratory
California Institute of Technology

Prepared Under Contract No. NAS 7-100
National Aeronautics & Space Administration

CONTENTS

I. Introduction	1
II. Experimental Apparatus and Techniques	2
A. Engine	2
B. Instrumentation Provisions	5
C. Firing Procedure	6
III. High-Response Instrumentation	7
A. Description of System	7
B. Environmental Protection	8
C. Dynamic Response	9
D. Calibration Techniques	10
IV. Results	10
V. Discussion of Results	16
A. Data Validity	16
B. Interpretation of Results	18
VI. Summary of Results	20
Nomenclature	21
References	22

FIGURES

1. 20,000-lb-thrust engine and components used for resonant combustion measurements	3
2. 20,000-lb-thrust engine used in resonant combustion program, mounted on test stand (ETS "B" stand)	4
3. Face of RMIR Injector No. 5 as used for resonant combustion program	4
4. 20,000-lb-thrust engine high-frequency-response instrumentation locations	5
5. High-frequency pressure transducers installed on chamber wall of 20,000-lb-thrust engine	6
6. Engine firing profile to obtain resonant combustion measurements	6

FIGURES (Cont'd)

7. Disassembled bomb device used during resonant combustion program	7
8. Pressure compensated transducer shockmount	8
9. Kistler installation in injector face plate	8
10. Dynamic evaluation of instrumentation system	9
11. Typical pressure distribution along the chamber wall vs time during resonant combustion, RMIR Injector No. 5 with SFNA plus Corporal fuel	11
12. Typical pressure distribution across the injector radius vs time during resonant combustion, RMIR Injector No. 5 with SFNA plus Corporal fuel	12
13. Comparison of pressure vs time records of typical resonant disturbance as recorded by oscilloscope and magnetic tape	13
14. Intersection of resonant combustion wave with chamber boundary, RMIR Injector No. 5 with SFNA plus Corporal fuel	14
15. Resonant combustion pressure amplitude vs chamber boundary position, RMIR Injector No. 5 with SFNA plus Corporal fuel.	15
16. Acceleration effects in the output of a Kistler 603A transducer.	16
17. Comparison of transducer thermal drift rates during resonant combustion	17
18. Comparison of transducer outputs: shock tube tests and resonant combustion.	18
19. Chamber wall damage after prolonged exposure to resonant combustion	19

ABSTRACT

A single, high-amplitude pressure wave rotating with supersonic velocity about the combustion chamber axis has been observed during the resonant (oscillatory) combustion mode of several liquid rocket research engines. The occurrence of this very steep-fronted disturbance has led to the investigation of the applicability of a rotating detonation-like wave concept to explain the phenomenon. Results of a portion of the experimental phase of the investigation are presented showing the chamber boundary pressure distribution associated with resonant combustion exhibited by one of these engines. The engine was operated with nitric acid and aniline/furfuryl alcohol propellants at a nominal thrust of 20,000 lb and 300 psia chamber pressure.

The pressure distribution was obtained by several simultaneous high-frequency-response measurements across the radius of the injector face and along the length of the 11-in.-diameter cylindrical chamber. The pressure-wave-to-chamber-wall intersection was found to curve in the direction of wave rotation with the nozzle end of the intersection leading the injector end in excess of 40 deg circumferentially. The wave-to-injector-face intersection was found to be non-radial and to extend into the central area of the face — though the definition of the intersection was poor in this area.

The observed pressure ratio across the wave front (ratio of peak-to-minimum pressures during a wave rotation period) varied along the chamber wall from in excess of 20:1 near the injector to 4:1 near the nozzle entrance. The pressure ratio at the face varied from approximately 20:1 in the outer half radius to less than 4:1 near the center. The nonsymmetrical wave exhibited a rise time of less than 3 μ sec at certain boundary locations.

A discussion on the performance of the high-response instrumentation system is also presented. The principal areas of this discussion include:

1. Results of tests to evaluate the uncooled quartz transducer and the 80-kcps-response FM analog record/playback equipment.
2. Advanced techniques for minimizing the effects on transducer output of temperature and vibration along with a discussion of the effects of these protective techniques on basic transducer frequency response.
3. Results of shock tube and rocket engine tests as applicable to the transducer system evaluation.

I. INTRODUCTION

The liquid rocket combustion processes must, in general, proceed in such a manner that the operating characteristics of the engine fall within design specifications dictated by the engine's propulsive mission. While never truly steady in time, those processes and their influence on the operation of a *propulsively useful* engine can be included in some quasi-steady-state behavior such that the thrust-producing performance level, heat rejected to the chamber and nozzle boundaries, combustion-excited mechanical vibration spectrum, thrust vector orientation, etc., are either analytically predictable or empirically reproducible.

Rather frequently, however, a tendency to shift from this "steady" mode of operation to certain "unsteady" modes is observed. These unsteady modes are characterized by fluctuations in the combustion processes which, if of sufficient amplitude to shift the engine's operating characteristics outside the design specifications, may preclude the attainment of the propulsive mission and, indeed, may precipitate the destruction of the engine. Combustion modes having these potentials are commonly called "combustion instability modes."

One of the most significant and experimentally observable manifestations of the rocket combustion processes is the combustion chamber pressure, and invariably this parameter is observed to fluctuate in some manner whenever the so-called instability modes are present. Those modes which yield sustained pressure fluctuations exhibiting periodicity are termed resonant or oscillatory modes.

One mode of resonance which has become increasingly predominant as chamber diameter, propellant mass flux (propellant flow rate per unit of chamber cross section) and combustion efficiency have increased is commonly identified as "spinning-tangential instability." This terminology is derived from the fact that a pressure disturbance rotates circumferentially about the chamber wall. Analytical models to describe this phenomenon have heretofore been based upon considering the chamber and nozzle (to the throat section) as a resonating acoustical cavity filled with combustion product gas. The resonant pressure disturbance (or the associated gas velocity disturbance) is presumed to interact on the combustion processes with a phase relationship such that the pressure disturbance is sustained by the difference between

the chemical and damping energies imposed on the vibratory gas system.

A particularly severe example of this rotating mode of resonance was encountered in the experimental operation of several engines at this laboratory during a recent injection research program (Ref. 1).¹ The severity of the phenomenon in its fully developed form was dramatically affirmed by heat transfer rates to the chamber wall near the injector: an order of magnitude greater than those observed during steady combustion (Ref. 2). Firing durations under these conditions for greater than half a second generally resulted in a complete burn-through of the 3/4-in.-thick steel chamber wall and in substantial thermal and erosion damage to the injector face. That this destructive combustion mode was no "fluke" was verified by the fact that it was consistently observed whenever injection schemes yielding high combustion efficiency (95-98%) were utilized with the 11-in.-diameter, 20,000-lb-thrust engines of that program.

Ultimately the transition from steady to resonant combustion in those engines was eliminated by the incorporation of baffles on the injector face. However, without those control devices chamber pressure perturbations such as randomly rough combustion or hard starting transients always resulted in a self-excited, nearly spontaneous transition to the full amplitude of the resonance.

As a result of the analysis of several simultaneously recorded chamber pressure measurements which were made in the course of the RMIR program, it was concluded that the high-pressure amplitude and steep-frontedness of the disturbance and the spontaneity of transition to the fully developed resonance were not reconcilable with the classical acoustical models used to explain spinning tangential instability even though the period of the disturbance did approximate the predictions of those models. This conclusion led to the hypothesis of a "rotating detonation-like wave" concept to explain the phenomenon (Ref. 1). This concept is similar to that described by Krieg (Ref. 3); however, several other investigators have also suggested the significance of detonative processes to rocket combustion instability (Refs. 4-7).

¹The so-called Rocket Motor Injector Research (RMIR) program

While an analytical description has not yet been achieved, the concept envisions a shock wave which is rotating within a sensitive reaction zone near the injector and which is continually sustained by a nearly instantaneous chemical energy release of the propellant mass through which the wave passes. The wave is bounded by the chamber wall and injector face and extends inward from the wall some distance short of the center of the chamber. The wave front is inclined to the chamber longitudinal axis and may not be oriented radially in any plane of chamber cross section.

Thus, during each rotation the wave sweeps through the same annular space where the propellants have been continuously replenished (from the injector) during the period of wave rotation. The strength of the wave (pressure ratio across the front) is presumed to be a function of the net energy released by the reacting propellants immediately behind the wave front and hence should be strongly dependent on the unreacted propellant mass present in the path of the wave, the mixing efficiency of the injector, and the degree of coupling between the wave environment and the unreacted propellants. The particle motion of the burned gases following the passage of the wave follows some helical (perhaps vortical) path down the length of the chamber and out through the nozzle.

The ultimate objective of this Laboratory's current resonant combustion program is to determine experimentally and analytically the applicability of this concept to explain the high-amplitude, high-frequency

combustion pressure oscillations associated with the so-called spinning tangential instability. It is believed that a better understanding of the significant processes involved in a fully developed form of the resonance will lead to an appreciation for the requirements of a propulsion system design which will avoid the transition from steady to resonant combustion and thus provide stability for the system.

The purpose of this report is to present the results of an initial series of experiments which were conducted as a first step toward this objective. These experiments were intended to provide further definition of the chamber boundary pressure distribution produced during fully developed resonant conditions by one of the combustion systems which had been utilized in the RMIR program. This was accomplished by increasing the number and quality of simultaneous pressure measurements beyond that which had been achieved in the former program. Thus, a necessary adjunct to the combustion experiments was the development of a suitable high-response instrumentation system. Some pertinent results of the development and evaluation of this system will be discussed.

The engine was operated without injector baffles but in such manner that self-excited resonance was avoided (i.e., steady combustion was relatively noiseless and the starting transients were controlled to provide an essentially monotonic chamber pressure start transient). The transition to resonance was induced by a combustion pressure pulse which was provided by means of a bomb device.

II. EXPERIMENTAL APPARATUS AND TECHNIQUES

A. Engine

The 20,000-lb-thrust engine used in these experiments is shown schematically in Fig. 1. The assembly consisted of an uncooled, heavy-walled combustion chamber/nozzle assembly and an injector design optimized to achieve a nearly uniform propellant mass and mixture ratio distribution within the combustion chamber. Figure 2 shows the complete engine installed on the test stand nearly ready for firing.

The 11.046-in.-diameter, 16.445-in.-long cylindrical chamber had a wall thickness of 0.75 in. and was fabricated from mild steel. A clamped flange arrangement at the chamber-to-injector junction permitted the chamber to be installed at continuously variable angular orientations with respect to the injector.

A copper nozzle with a nominal throat diameter of 7.756 in. provided an engine contraction ratio of 2.028.

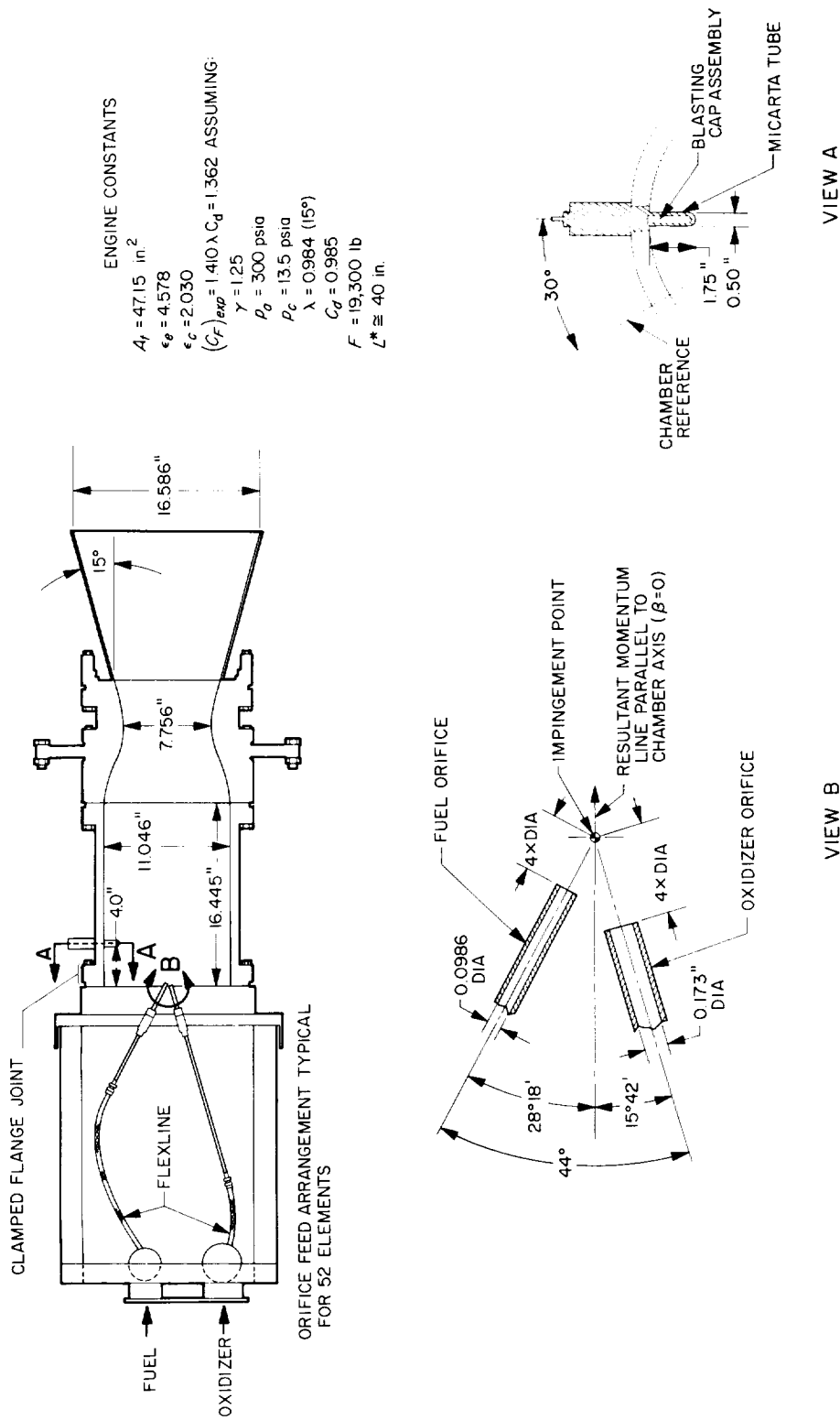


Fig. 1. 20,000-lb-thrust engine and components used for resonant combustion measurements

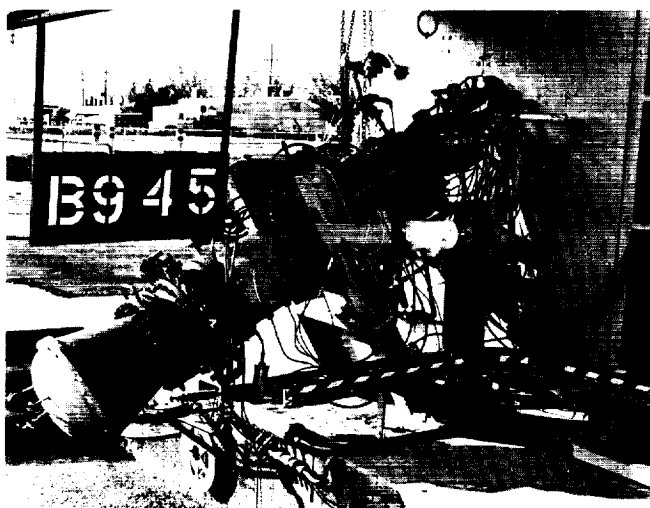


Fig. 2. 20,000-lb-thrust engine used in resonant combustion program, mounted on test stand (ETS "B" stand)

A nozzle expansion ratio of 4.578 was obtained through the use of a steel expansion section with an exit diameter of 16.586 in. This expansion provided a slightly over-expanded nozzle exit plane pressure of 9.7 psia at the design chamber pressure of 300 psia (the prevailing test site ambient pressure was 13.5 psia). Other pertinent engine constants are listed in the table included on Fig. 1.

The injector assembly, designated RMIR Injector No. 5, consisted of 52 identical unlike impinging elements which were designed to satisfy the mixing uniformity criterion (Ref. 8) for the SFNA² and *Corporal* fuel³ propellant combination at a mixture ratio (w_{ox}/w_f) of 2.80. This criterion states that for the most uniform mixture ratio distribution throughout a spray formed by two unlike impinging liquid streams, the product of the velocity-head ratio and diameter ratio for the two streams is unity. The element geometry shown in Fig. 1 is the consequence of satisfying that requirement with the above propellants and mixture ratio. The injection velocities are 138 and 87 ft/sec, respectively, for the fuel and oxidizer jets.

² SFNA (stabilized fuming nitric acid) consists of a mixture of the following compounds with percentage by weight as noted: 81.3–84.5% HNO₃; 14.0±1.0% NO₂; 2.5±0.5% H₂O; 0.6±0.1% HF.

³ *Corporal* fuel consists of a mixture of the following compounds with percentage by weight as noted: 46.5±0.2% furfuryl alcohol (C₄H₃OCH₂OH); 7.0±0.2% N₂H₄; 1.5% max H₂O; 0.7% max impurities; remainder, aniline (C₆H₅NH₂).



Fig. 3. Face of RMIR Injector No. 5 as used for resonant combustion program

The arrangement of the 52 elements in the flat face plate is shown photographically in Fig. 3. This arrangement provided a nearly uniform axial mass distribution of the injected propellants throughout the combustion volume. Note, however, that some local nonuniformity did exist in the proximity of the chamber wall by virtue of the nonsymmetrical element orientation with the wall surface.

Controlled and reproducible hydraulic properties of the unlike impinging streams were assured by the incorporation of 100-diameter-length orifices constructed of smooth-bore tubing. The fully developed turbulent flow and large friction loss associated with these long orifices also minimized maldistributions from the supply manifold and attenuated coupling effects between the supply pressure and combustion pressure oscillations.

While this engine has previously demonstrated an essentially constant relative combustion performance of 98% (based on equilibrium flow) when operated over the mixture ratio range of 1.9 to 3.2 with the SFNA + *Corporal* fuel propellants, the nominal design mixture ratio (2.80) was used for these experiments. Under these conditions the RMS value of chamber pressure fluctuations during the "steady state" combustion mode is less than 1 psi.

Further details of the design, construction and performance characteristics of the engine are contained in Refs. 9-11.

B. Instrumentation Provision

Provisions for installing a total of eighteen Kistler^{*} pressure transducers were incorporated on the injector

^{*}Manufactured by Kistler Instrument Co., Clarence, New York.

face and chamber walls as shown in Fig. 4. Five of these transducers were located on the face on radii of 0.78, 1.96, 3.22, 4.13, and 4.82 in. at clockwise angular positions of 320, 277, 272, 270, and 268 deg, respectively, from an assigned injector reference (as viewed from the nozzle end of the engine).

The remaining thirteen Kistler mounting provisions were located on the chamber wall. These were arranged along two longitudinal rows of six transducers each and

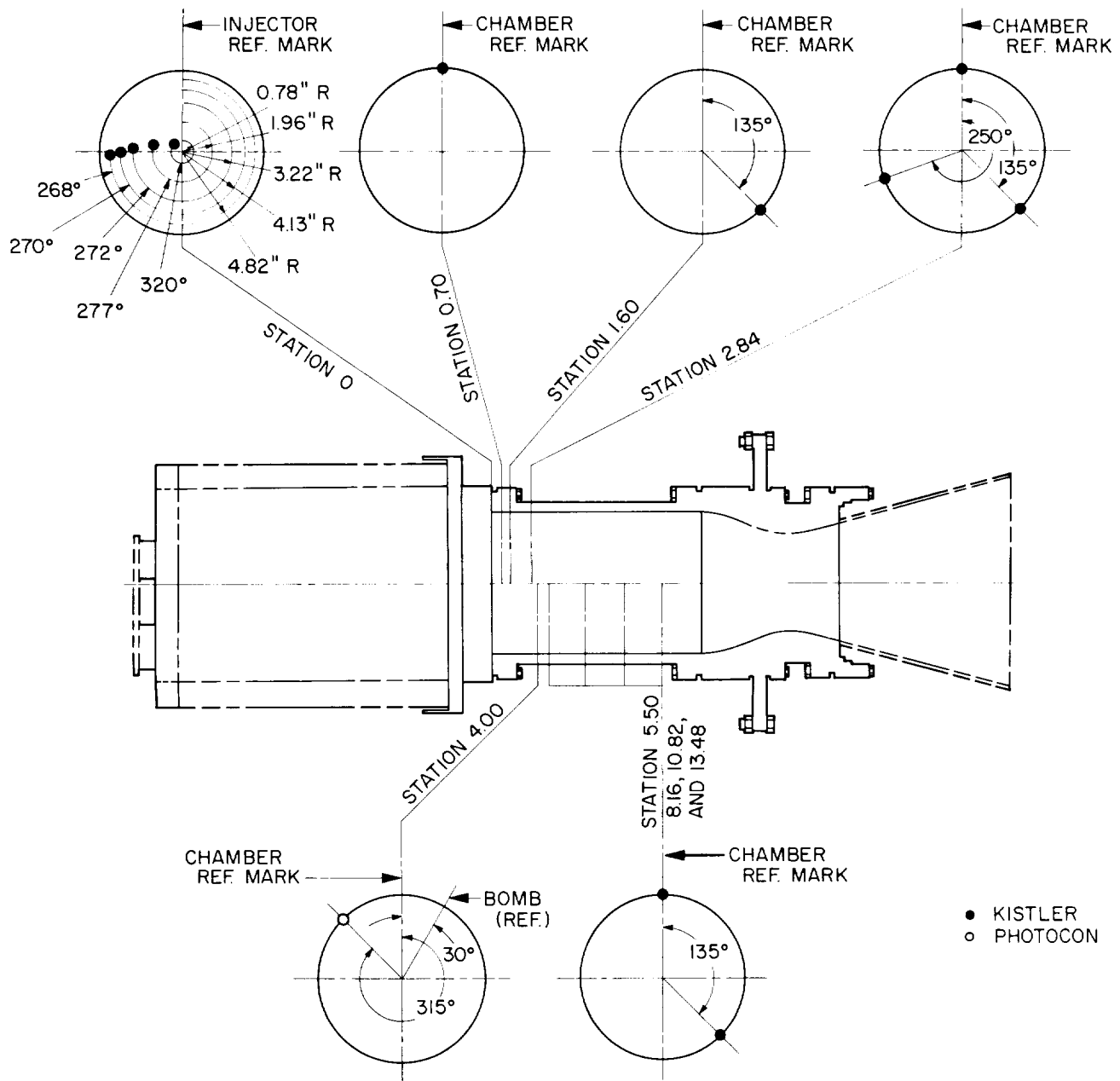


Fig. 4. 20,000-lb-thrust engine high-frequency-response instrumentation locations

at one location displaced circumferentially from either row. One of these rows lay along an assigned chamber reference while the other lay 135 deg clockwise (again as viewed from the nozzle). Each row consisted of five transducer locations at common axial stations 2.84, 5.50, 8.16, 10.82, and 13.48 in. from the injector face. Additionally, the chamber reference row contained a location at 0.70 in. while the other row (135 deg clockwise) contained one at 1.60 in. The singularly displaced location was located at the 2.84-in. station but at 250 deg clockwise from the chamber reference.

Supplementing the Kistler provisions, one Photocon⁵ transducer mounting boss was located 4.00 in. from the face at 315 deg clockwise from the chamber reference.

The external appearance of the chamber instrumentation as installed on the engine is shown in Fig. 5.

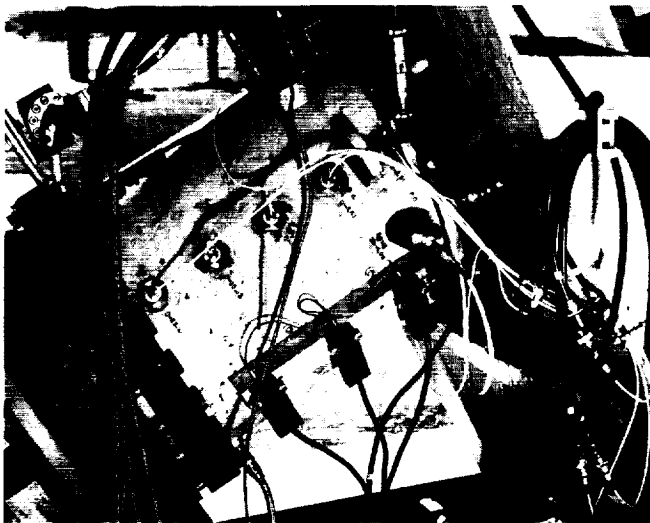


Fig. 5. High-frequency pressure transducers installed on chamber wall of 20,000-lb-thrust engine

In order to monitor the steady-state performance of the engine and propellant feed system, the standard low-response measurements of chamber pressure, flow rates, thrust, injector manifold pressure and propellant supply pressure were made for each firing. These data were recorded on digital magnetic tape and were subsequently reduced to engineering units and/or performance by means of a machine computer.

⁵Manufactured by Photocon Research Products, Pasadena, California.

C. Firing Procedure

The duration of the engine firings was limited to very short times in order to minimize the thermal effects on the pressure transducers. A typical firing profile as characterized by chamber pressure is illustrated in Fig. 6. Each firing consisted of an approximate 300-msec period of "smooth" combustion, which allowed sufficient time to proceed through the engine starting transients and for flow rates (hence operating chamber pressure) to achieve quasi-steady-state values. At the end of this period a bomb pulse was electrically initiated which precipitated a transition to the resonant combustion mode. The firings were terminated after approximately 100 msec of resonance by an electrically operated sequence timer.

The installation of the bomb device on the chamber wall is shown in Fig. 1. The bomb components are illustrated in Fig. 7. These parts consisted of a 13.5-grain high-explosive charge in the form of a blasting cap⁶, a Micarta tube to protect the explosive from the combustion environment and a supporting fixture. When installed in the chamber, the end of the blasting cap was located approximately 1 3/4 in. inside the chamber and 4 in. from the injector face.

The initial pressure wave generated by the bomb explosion is presumed to have progressed omni-directionally into the combustion volume. Reliable resonance initiation was obtained throughout these experiments with this particular charge size.

⁶Designated Model E-83 by the manufacturer, E. I. Dupont De-Nemours and Co., Inc., Wilmington, Delaware.

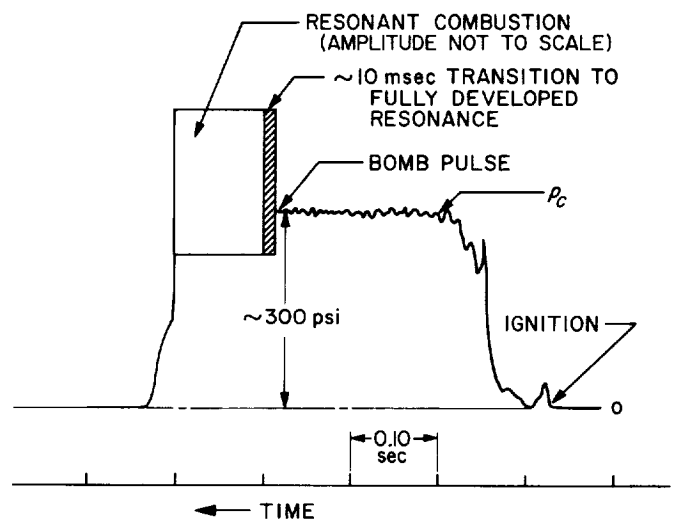


Fig. 6. Engine firing profile to obtain resonant combustion measurements

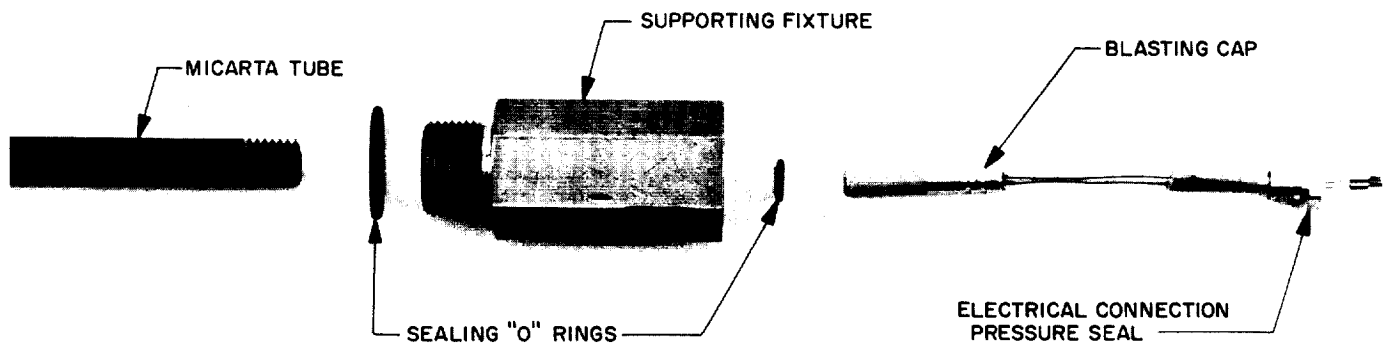


Fig. 7. Disassembled bomb device used during resonant combustion program

III. HIGH-RESPONSE INSTRUMENTATION

A. Description of System

In order to fulfill the objectives of these experiments the following instrumentation requirements were initially specified:

1. Measurement of both AC and DC amplitude components from at least six chamber boundary locations simultaneously. Pressure waves with frontal rise times of less than $2 \mu\text{sec}$ were expected.
2. Resolution of the phase relationship between the several measurements to within $2\frac{1}{2}$ deg at the chamber circumference.
3. Satisfactory operation for periods of at least 150 msec under environmental conditions of at least 12 BTU/in.²-sec heat transfer and at least 2000-g peak vibration amplitude.
4. Satisfactory operation at a test stand area with the recording area located at a distance of 500 ft from the test stand.

These requirements approach the state-of-the-art for rocketry instrumentation; hence, the development of a suitable integrated system was of paramount importance. The system to be described is one result of a continuing program conducted by this Laboratory's Instrumentation

Section to provide these measurement capabilities (Refs. 12, 13). Efforts were concentrated on the development of an uncooled, shock-mounted installation of the Kistler quartz-crystal transducer because of the high mechanical natural frequency and relatively small size (0.21-in. diaphragm diameter) of the transducer.

As used for these experiments, a typical Kistler channel of instrumentation consisted of a Model 603A transducer, Model 566 charge amplifier (located in close proximity to the test stand) and approximately 500 ft of RG59 triaxial cable which coupled the amplifier output to a 14-channel CEC VR2600 tape recorder⁷.

All the high-response measurements were recorded on the magnetic tape in the FM mode at 120-ips tape speed. Sufficient time expansion to permit detailed analysis of the recorded data was achieved by playing back the data at reduced tape speeds into a galvanometric oscillograph. This record/playback technique resulted in an effective paper speed, continuously variable, of from less than 1 to 12,800 ips ($83 \mu\text{sec/in.}$ maximum time resolution).

⁷ Manufactured by Consolidated Electrodynamics Corporation, Pasadena, California.

B. Environmental Protection

The effect of high chamber wall vibration levels on transducer output during resonant combustion conditions required that transducers located thereon be isolated from this environment. Shown in Fig. 8 is a cross-section of the pressure-compensated shockmount which was used for this purpose together with its vibration isolation characteristics. The transducer is supported in an adapter which is isolated from the chamber wall by silastic "O" rings. The softness of the isolation is maintained by the pressure-balanced feature of the design whereby chamber pressure is ported to act on an internal area equal to the exposed chamber-side area.

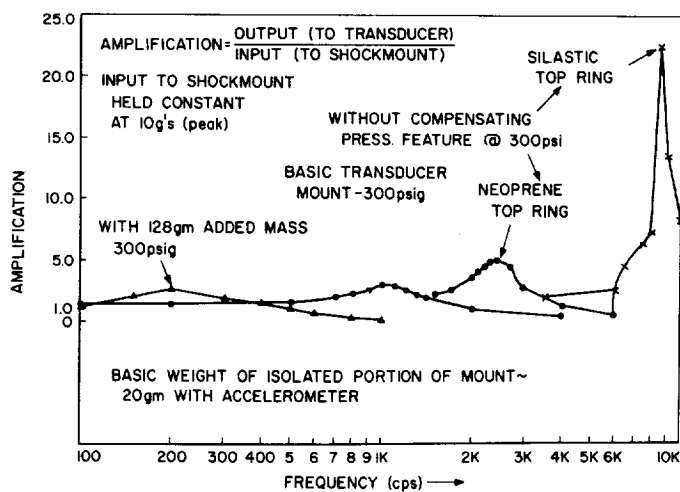
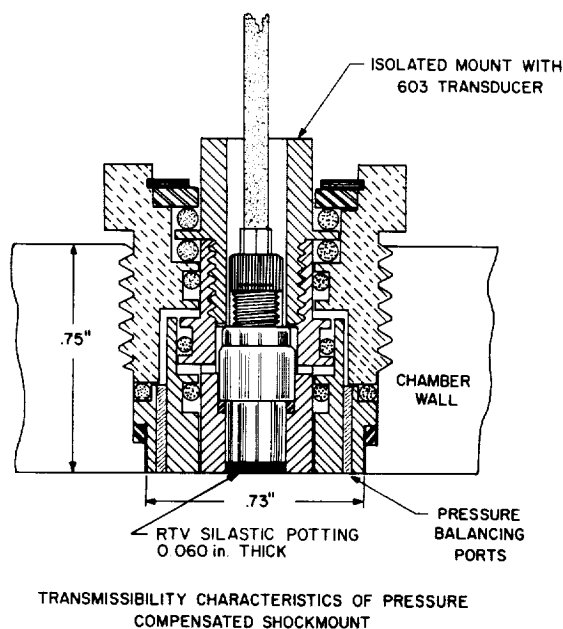


Fig. 8. Pressure compensated transducer shockmount

The isolation curves show the characteristics obtained for two values of adapter/transducer mass, 150 and 20 g. The resonant points are approximately 200 and 1000 cps, respectively. The mount currently in use has a mass of approximately 60 g and a resonance of 600 cps and therefore furnishes appreciable isolation at the dominant combustion pressure frequencies which have been encountered to date, i.e., from 1500 to 2500 cps. The curve to the right on the plot shows the significance of the pressure compensation by showing the loss of isolation when the pressure ports are plugged.

Unfortunately, the space available amongst the injector orifices prohibited the installation of shock-mounted transducers in the injector face. It is noted, however, that little evidence of vibration output has been observed in the face measurements. It is felt that the 2½-in.-thick face plate reduces the level of vibration imposed on the transducers to a negligible amplitude. A typical face transducer installation is shown in Fig. 9.

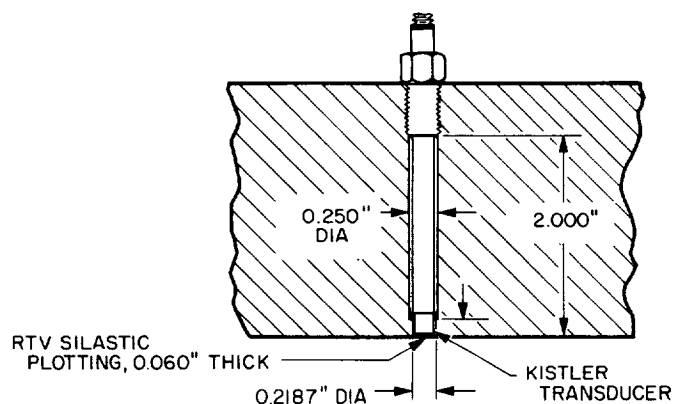


Fig. 9. Kistler installation in injector face plate

The high heat transfer rates encountered during resonant combustion cause high-response measurements to be troublesome to perform. The selection of an uncooled transducer configuration, seemingly in contradiction to these conditions, stemmed from the apparent difficulty of incorporating standard cooling schemes (based on water or gas flow) and concomitantly retaining a maximized dynamic response. Thermal protection was obtained, however, from an ablative or insulation technique which consisted of recessing the diaphragm approximately 0.060 in. from the chamber boundary surface and filling the resulting cavity with a high-temperature ablative material such as RTV 560 silastic rubber*. In this manner

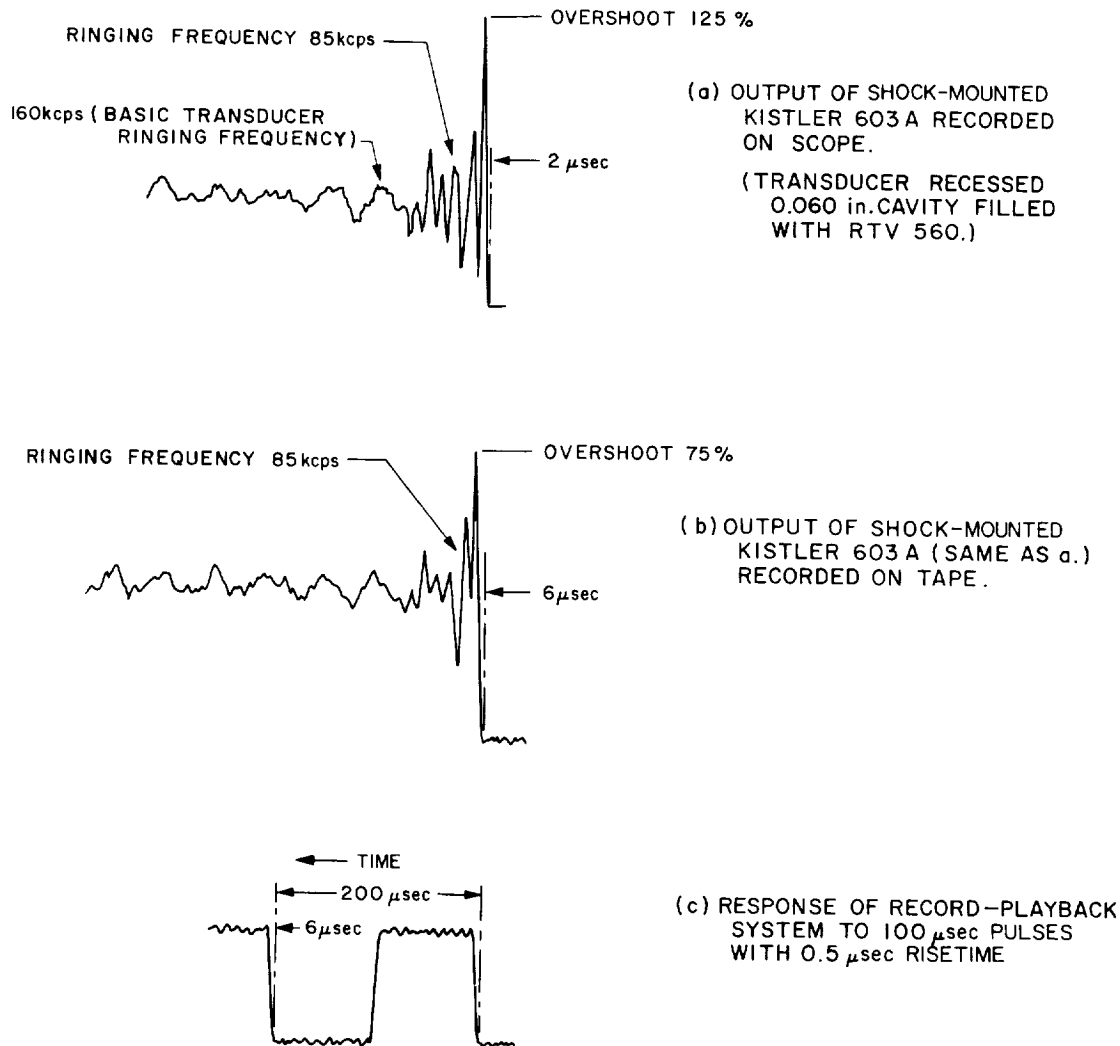
*Manufactured by General Electric Silicone Products Department, Waterford, New York.

transducer durability was improved and thermal effects were reduced to a tolerable level while it could be shown that dynamic response was only slightly affected.

C. Dynamic Response

A shock tube was employed as the basic "laboratory" tool for the evaluation of the dynamic response of the

instrumentation. The output of the system to be evaluated when exposed to the step change in pressure resulting from either "end" or "side shots" of the tube was recorded by oscilloscope photography or magnetic tape. In the latter instance the test data were recorded in a manner similar to that used to record combustion data. These tests provided information as to transducer rise time, overshoot and ringing frequency; pointed up dis-



NOTES:

1. TRACE (a) AND (b) ARE RESPONSE OF 603A TRANSDUCERS TO END-MOUNTED SHOCK-TUBE TESTS. HIGH OVERSHOOT AND LOW (85 kcps) RINGING FREQUENCY ARE CAUSED BY RTV 560 FILLED CAVITY IN FRONT OF DIAPHRAGM.
2. TEST SIGNAL FOR TRACE (c) INTRODUCED AT TAPE RECORDER INPUT
3. SAME TIME SCALE ALL TRACES

Fig. 10. Dynamic evaluation of instrumentation system

crepancies between transducers; evaluated the effects of transmission line lengths and charge amplifier gain settings; and provided a method for comparing overall system response characteristics with records made by the same system during an actual engine firing.

Some typical examples of these laboratory evaluations are shown in Fig. 10. Trace (a) is the response of a transducer/charge amplifier system to an end shot as recorded on an oscilloscope in the shock tube laboratory using relatively short transmission lines. Trace (b) is the output of the same transducer/amplifier system as recorded on tape using 500 ft of transmission lines. The recorded rise times are 2 μ sec and 6 μ sec, respectively. Note that the higher frequency oscillations (above 80 kcps) are significantly attenuated in the tape record (trace b) but are still quite evident; thus the usable response of the tape recorder exceeded 80 kcps. A further evaluation of the record/playback system is shown in trace (c), which depicts the results of recording a series of electronically generated square wave pulses having less than 0.5- μ sec rise time. The recorded 6- μ sec rise time duplicates that shown in trace (b) and hence is apparently the limiting rise time of the recorder/playback electronics. It is noted that the recording electronics

overshoot is essentially null (trace c) and that this is the result of using Gaussian-type filters in the recorder reproduce amplifiers.

D. Calibration Techniques

Prior to each firing, all the Kistler systems were calibrated to determine their static sensitivities and dynamic responses. Static calibrations consisted of pressurizing an individual system with a dead-weight tester as a check on linearity and hysteresis. At the same time the respective charge amplifiers were examined for zero-drift and noise. After assembling the transducer/shockmount assemblies and potting the diaphragm cavities with silastic material, the assemblies were dynamically tested on the shock tube.

After installation on the motor, such tests as cable disconnection and chamber pressurization insured proper channel identification and verified the calibration sensitivity, output polarity, noise level and drift. Known amplitude square and sine wave calibration signals were introduced at the charge amplifier and recorded on tape to provide the recording sensitivity.

IV. RESULTS

Portions of typical pressure vs time records obtained during fully developed combustion resonance (25 msec after the bomb pulse) are illustrated in Figs. 11 and 12, which show, respectively, a set of simultaneous measurements down the length of the chamber and across the injector radius. These records were obtained during two engine firings for which the chamber-to-injector angular orientation was maintained constant. The resulting geometric orientation of the several measurements is shown schematically on the right-hand side of each figure. In the interest of clarity, duplicate measurements made during each firing are not shown. All traces are DC analog records of Kistler outputs, except the channel marked P₃₁₅₀₄₀₀, which was a Photocon measurement.

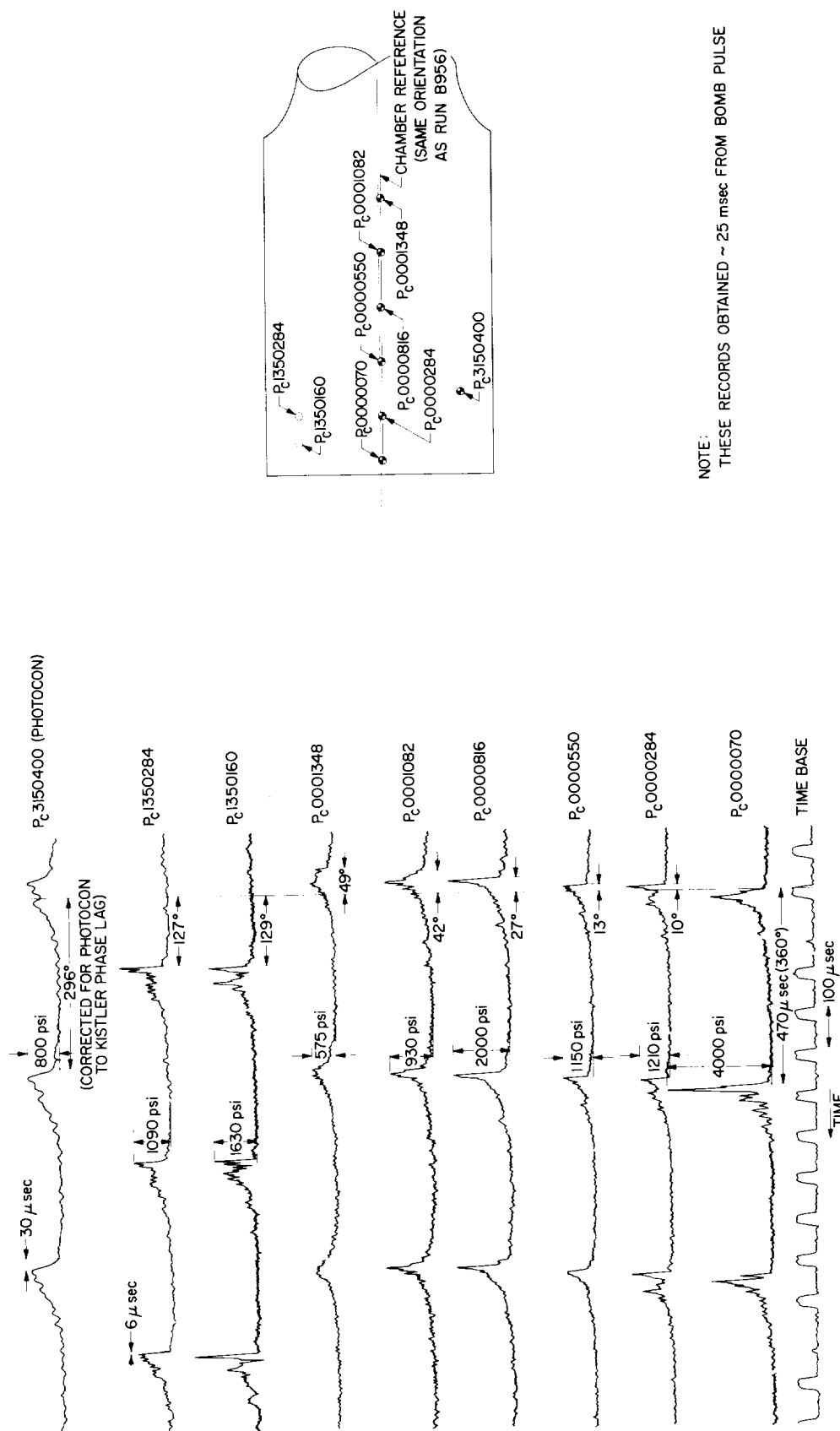
The salient transient features of the resonance as typified by these records may be summarized as follows:

1. A single disturbance is traveling in a clockwise rotational direction as viewed from the nozzle end

of the chamber. This direction of travel is deduced from the correspondence between the recorded phase displacement and the transverse geometric displacement of the P₁₃₅₀₂₈₄ and P₀₀₀₀₂₈₄ measurements as shown in Fig. 11. The phase displacements apparent in the measurements along the longitudinal reference line are indicative of the shape of the disturbance-to-wall intersection.

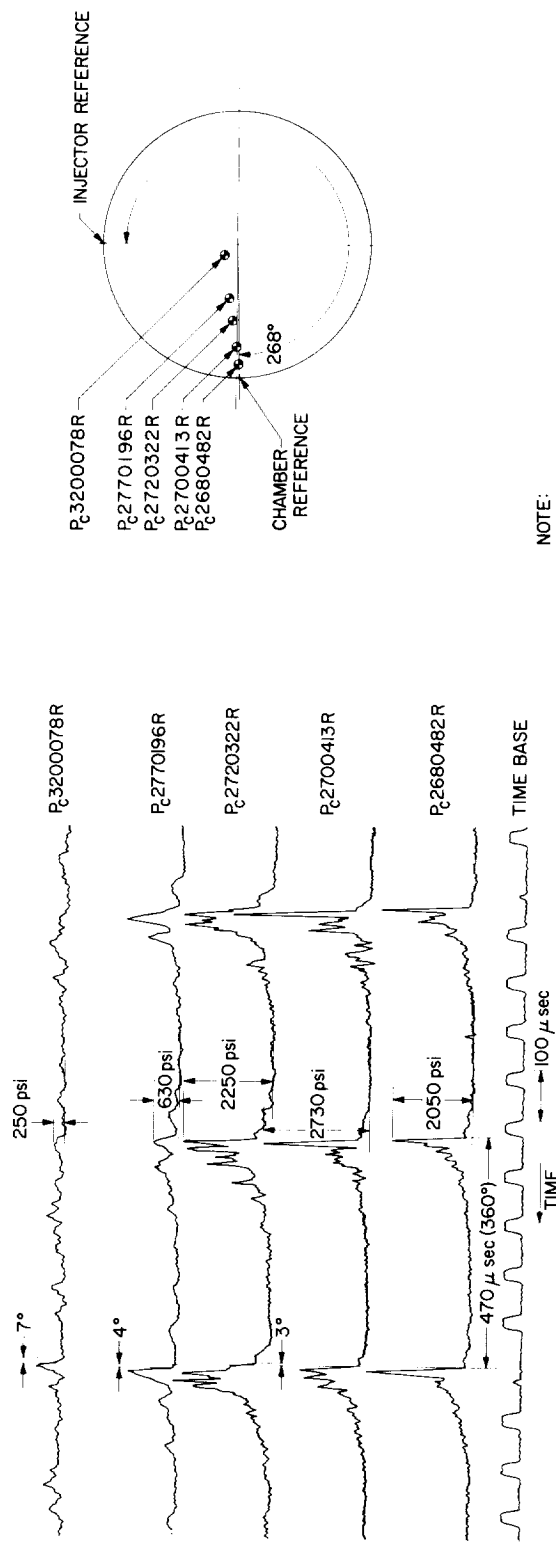
2. The period is essentially identical for all measurement locations on the face and wall. The 470- μ sec periods indicated for the P₀₀₀₀₀₇₀ (Fig. 11) and P_{2680482R} (Fig. 12) locations are typical. Variations in this period of as much as 10% were observed; however, the variations appeared to be random in occurrence.

Based on the 470- μ sec period and the 11.046-in. chamber diameter, the tangential velocity of the disturbance-to-wall intersection is 6160 ft/sec. If a



RUN B958

Fig. 11. Typical pressure distribution along the chamber wall vs time during resonant combustion, RIMR Injector No. 5 with SFNA plus Corporal fuel



RUN B956

Fig. 12. Typical pressure distribution across the injector radius vs time during resonant combustion, RIMR Injector No. 5 with SFNA plus Corporal fuel

sonic velocity of 3500 ft/sec is assumed for the chamber gases (from the experimental steady-state performance of the engine), this intersection velocity corresponds to a Mach number of 1.76.

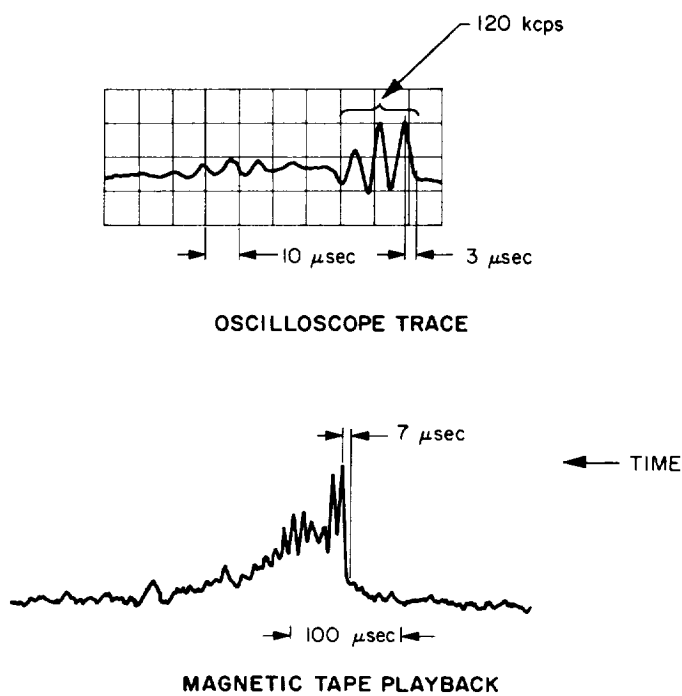
3. The peak amplitude of the disturbance varies with the location of the measurement. The greater amplitudes were observed near the injector end of the chamber wall and in the outer half-radius of the injector face.

Note that considerable amplitude variation is apparent for any particular location (the P.0000070 trace in Fig. 11 for example)—especially in the higher amplitude areas of the disturbance. No predominant periodicity or modulating frequency has been found for these variations; hence they appear to occur randomly in both time and amplitude.

4. The wave form of the disturbance, particularly at locations near the injector end of the chamber, consists of steep-fronted, spiked pulses which rise from a minimum to a peak amplitude in recorded times of approximately $6\text{ }\mu\text{sec}$. These pulses are in turn followed by an approximate $100\text{-}\mu\text{sec}$ period of time during which the amplitude decays to essentially the initial minimum pressure. Thus the entire disturbance passes a particular boundary location in less than 25% of its rotation period.

Near the nozzle end of the chamber and in the central area of the injector face, the disturbance becomes much less steep. In fact, at the innermost face measurement (P.3200078R of Fig. 12) the identification of a singular disturbance becomes almost impossible at times. Yet at different times the presence of the disturbance is clearly indicated at this location having substantial amplitude (albeit reduced steep frontedness) and the $470\text{-}\mu\text{sec}$ period.

Since the recorded $6\text{-}\mu\text{sec}$ rise time of the disturbance coincides with the maximum capability of the tape recorder system, an ancillary experiment was performed in order to further evaluate the steepness of the front. This experiment was performed by connecting the output of one of the Kistler transducers to an oscilloscope for one firing. The oscilloscope sweep was triggered by the output of a second Kistler. This trigger transducer was located on the chamber so that its output (as the resonant wave passed) synchronized the sweep with the pressure wave passage over the transducer whose output was to be recorded. The resulting oscilloscope record is depicted in Fig. 13, where it is compared with the dually recorded tape record of the same transducer. Note, however, that the two records are not necessarily of the same



NOTE THAT THESE RECORDS ARE NOT NECESSARILY OF THE SAME PRESSURE PULSE BUT WERE TAKEN DURING A SINGLE FIRING (B960) FROM THE OUTPUT OF SINGLE KISTLER TRANSDUCER LOCATED AT 0000284

Fig. 13. Comparison of pressure vs time records of typical resonant disturbance as recorded by oscilloscope and magnetic tape

pressure pulse, since the oscilloscope sweep time was not correlated with a particular time during the firing.

While the $3\text{-}\mu\text{sec}$ rise time indicated on the oscilloscope record corresponds closely to the travel time of the disturbance across the transducer diaphragm ($2.7\text{ }\mu\text{sec}$), it is noted that the disturbance transient excited what appears to be the 120-kcps natural mechanical resonant frequency of the transducer. This is substantial evidence that the $3\text{ }\mu\text{sec}$ is actually the limiting rise time of the measurement and that the actual pressure transient is shorter than this.

The instantaneous disturbance-to-chamber boundary intersection as deduced from records similar to those shown in Figs. 11 and 12 is shown in Fig. 14, where data from three different firings are presented. The "steady state" operating conditions at the time of the bomb pulse are shown on the figure, and although these conditions were not identical for each run, they were within 10% of the nominal design conditions of 300-psia chamber pressure and 2.80 mixture ratio. It is therefore

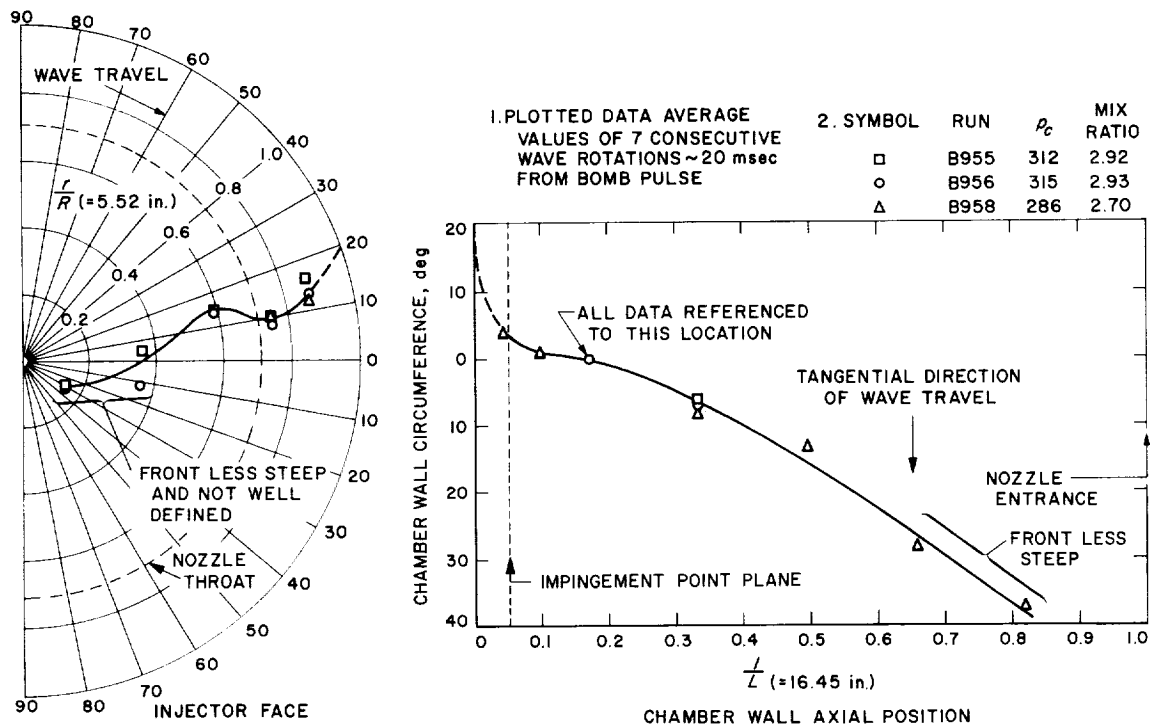


Fig. 14. Intersection of resonant combustion wave with chamber boundary, RMIR Injector No. 5 with SFNA plus Corporal fuel

presumed that the gross combustion behavior was essentially identical for each firing. The plotted data are average values taken over a total of 7 consecutive wave rotations. The variation from this average value for any individual rotation was generally less than ± 3 deg except for the two measurements nearest the injector center. Variations of ± 15 deg were common at these locations.

Examination of this figure shows that the intersection extends along the entire range of wall measurement locations and that a curvature in the direction of wave rotation is exhibited such that the nozzle end of the intersection leads the injector end in excess of 40 deg. The wave-to-injector-face intersection is nonradial and extends into the central area of the face, although, as previously mentioned, the definition of the intersection is poor in this area. In a manner similar to that of the wall intersection, the less steep-fronted portion of the face intersection (near the center) leads the better defined portions of the disturbance.

It is noted that there is a point of inflection in both the wall and face intersection curves in the proximity of the face and wall boundary junction (i.e., the "corner"

of the chamber) which results in a "steepening" of the intersection curves in this region. The lack of a pressure measurement in this corner prevents extending these curves to that point; however, the dashed lines show a possible extrapolation from the measured points.

The pressure amplitude distribution for these same three firings is summarized in Fig. 15, in which the amplitudes are presented in terms of the minimum and maximum pressure (p_{min} and p_{pk} , respectively) during a disturbance period and pressure ratio which is defined as $p_{pk} + 13.5/p_{min} + 13.5$ (where 13.5 is the test site ambient pressure to which the pressure transducer calibrations were referenced). Again these data represent average values (\bar{p}) taken over 7 consecutive wave rotations. As was noted previously, considerable random variation in the amplitude was observed from rotation to rotation—especially in the higher-amplitude areas of the disturbance. Maximum variations relative to the indicated averages are shown in Fig. 15.

The curves which are shown are intended to represent a mean curve through the combined data of the three runs. Obviously, considerable scatter is present in the data points. It is believed, however, that the trend of

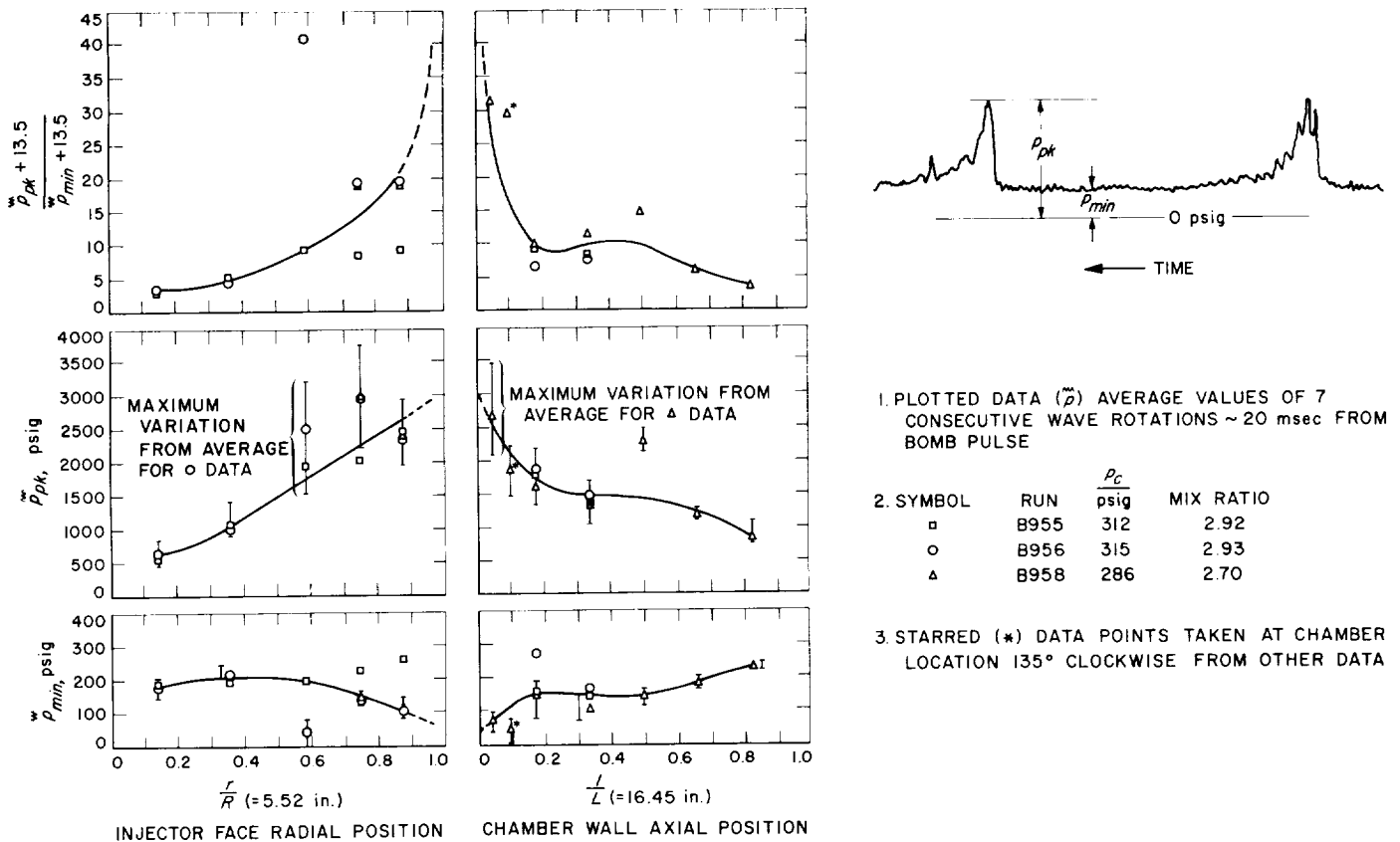


Fig. 15. Resonant combustion pressure amplitude vs chamber boundary position, RMIR Injector No. 5 with SFNA plus Corporal fuel

the pressure distribution is undeniable. Examination of these results shows that both the maximum values of \tilde{p}_{pk} and the minimum values of \tilde{p}_{min} occur near the corner of the chamber. Hence, the computed pressure ratio curve steepens sharply in this area. The lack of a corner measurement again prevents extending the plot to that location as observed data. If, however, the "measured" curve is extrapolated to this location it is fairly clear

that the observed pressure ratio would be in excess of 30:1.

The \tilde{p}_{pk} amplitudes decreased at locations towards the injector center and towards the nozzle end of the chamber; in general, \tilde{p}_{min} increased in these directions. The resulting pressure ratios at both locations diminished to approximately 4:1.

V. DISCUSSION OF RESULTS

A. Data Validity

The results which have been presented are measurements which are extremely difficult to perform. It is nearly impossible to assess quantitatively the effects of the environmental and transient conditions on the measurements owing to the difficulty in simulating them with anything short of the rocket engine itself. Thus, where it seemed feasible, an attempt was made to evaluate the performance of the instrumentation by comparing data from so-called standard instrumentation with data from non-standard or modified instrumentation.

It is felt that the effectiveness of the shockmount was particularly well demonstrated in this manner. This is illustrated in Fig. 16. Trace (a) shows the output of a Kistler 603A transducer shock-mounted on the chamber wall but with the transducer diaphragm blanked off so that it saw no pressure. The magnitude of the output due to vibration may be compared with trace (b), which depicts the output from a similarly blanked transducer but which was mounted rigidly on the chamber wall. The vibration output is attenuated by a factor of 10 in the case of the shock-mounted installation. A similar comparison between unblanked shock-mounted and hard-mounted transducers is shown in traces (c) and (d), respectively. Because the vibration sensitivity of the 603A transducer is inherently low, the amount of output due to vibration is difficult to measure from these latter records. The output of the hard-mounted transducer is definitely more noisy, however, and the vibration noise is estimated to represent some 20% of the signal. From these comparisons it is concluded that the shockmount effectively eliminated the effects of wall vibration on transducer output.

Available evidence indicates that transducer sensitivity is relatively unaffected by temperature unless the diaphragm becomes heated to the point of gross discoloration or burn-through. Zero-drift caused by crystal heating is, however, a significant problem. The use of the ablative coating has reduced this drift to an acceptable amount so long as the coating remains intact. The condition of the coating during an engine firing is, of course, dependent upon the ablation rate and firing duration as well as the achievement of an adequate bond between the ablative material and metal surface.

Figure 17 illustrates some drift rates exhibited during a typical engine firing. The entire firing has been com-

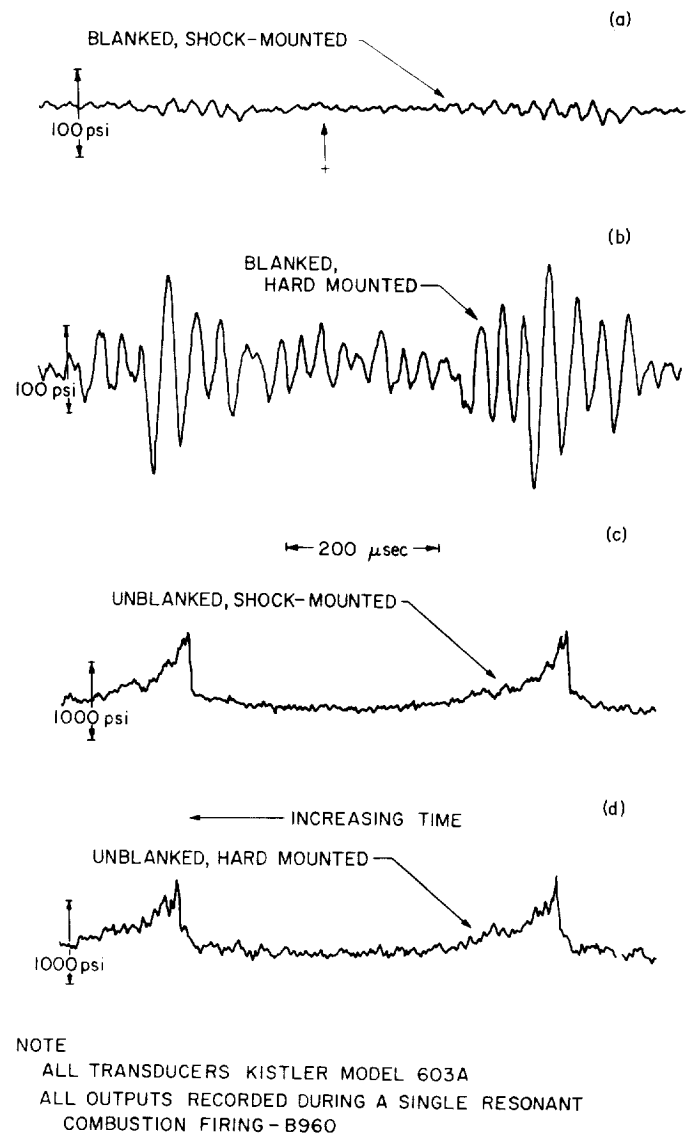
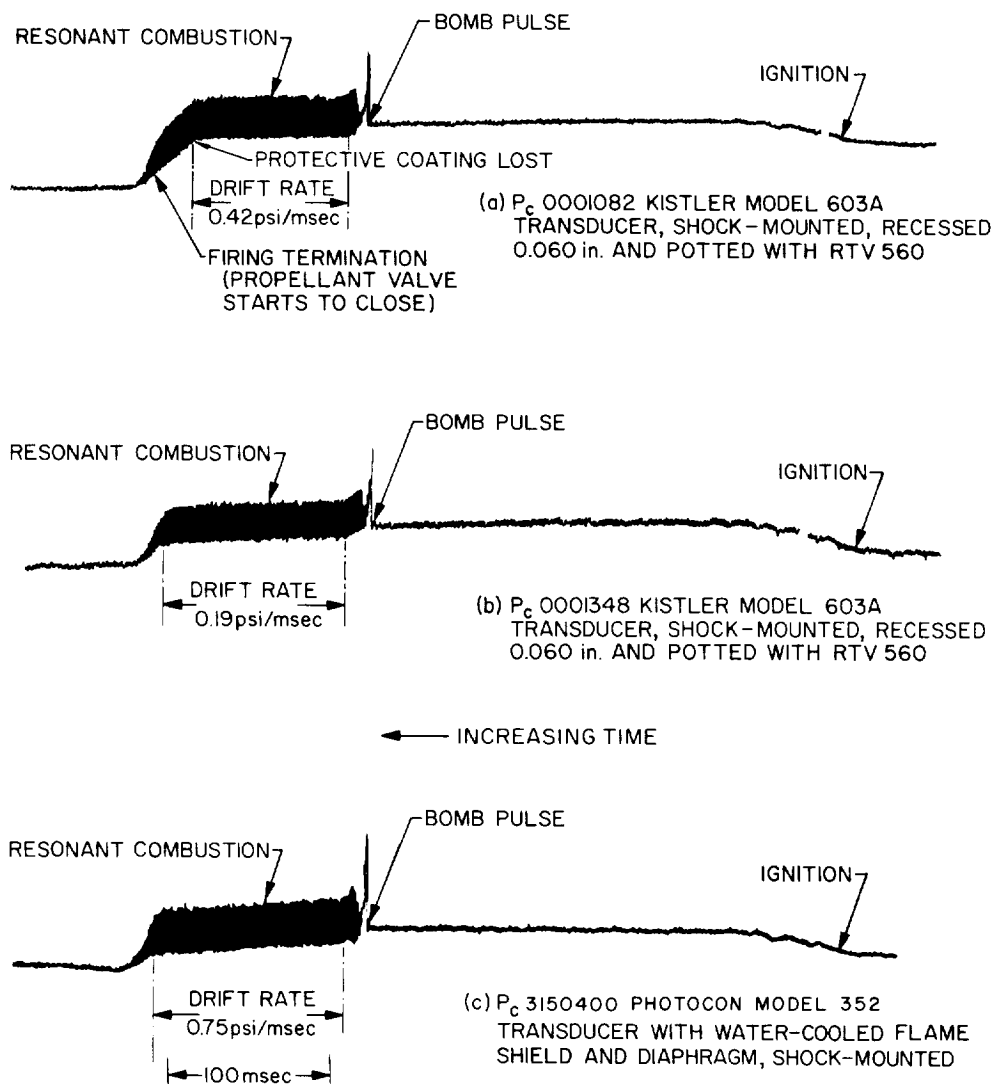


Fig. 16. Acceleration effects in the output of a Kistler 603A transducer

pressed into the space of a few inches on the record to better illustrate the drift. It is noted that these records were played back through a 1-kcps filter to eliminate unimportant (in this instance) high frequencies. Trace (a) illustrates the output of a transducer which lost its ablative coating just before the firing termination. Prior to the loss of thermal protection, the average drift rate was 0.42 psi/msec. Trace (b) shows a drift of 0.19 psi/msec throughout the entire period of resonance. This rate, typical of those measured when the protective coating remained intact, appears quite good considering the



NOTE: ALL TRACES RECORDED DURING A SINGLE FIRING (B948)

Fig. 17. Comparison of transducer thermal drift rates during resonant combustion

severe heat-transfer environment present. Trace (c) is the output of a Photocon Model 352 transducer with a water-cooled flame shield and diaphragm. Its drift rate prior to resonant conditions is lower than that of the Kistler; however, during resonant conditions its drift actually exceeds that of the uncooled transducers.

While these illustrations point up the relative success in using the uncooled transducer configuration, it must be noted that this was possible only because of the short firing durations, since the ablative coating has a very short life. Although corrections to the recorded data were applied to the data based on drift rate estimations obtained as just shown, it cannot be concluded that

thermal effects were negligible in the data. It is felt, however, that these effects were generally less than the errors caused by the dynamic response characteristics of the system which are discussed below.

Since all transducers were dynamically tested on the shock tube prior to each firing, it is interesting to compare a typical firing pressure record with the shock-tube test records. In this manner it is possible to gain at least a qualitative insight into the effects of the instrumentation dynamic response characteristics on the fidelity of the combustion data. In Fig. 18, trace (a) is the tape-recorded response of a transducer assembly end-mounted on the shock tube. The planar impingement of the shock

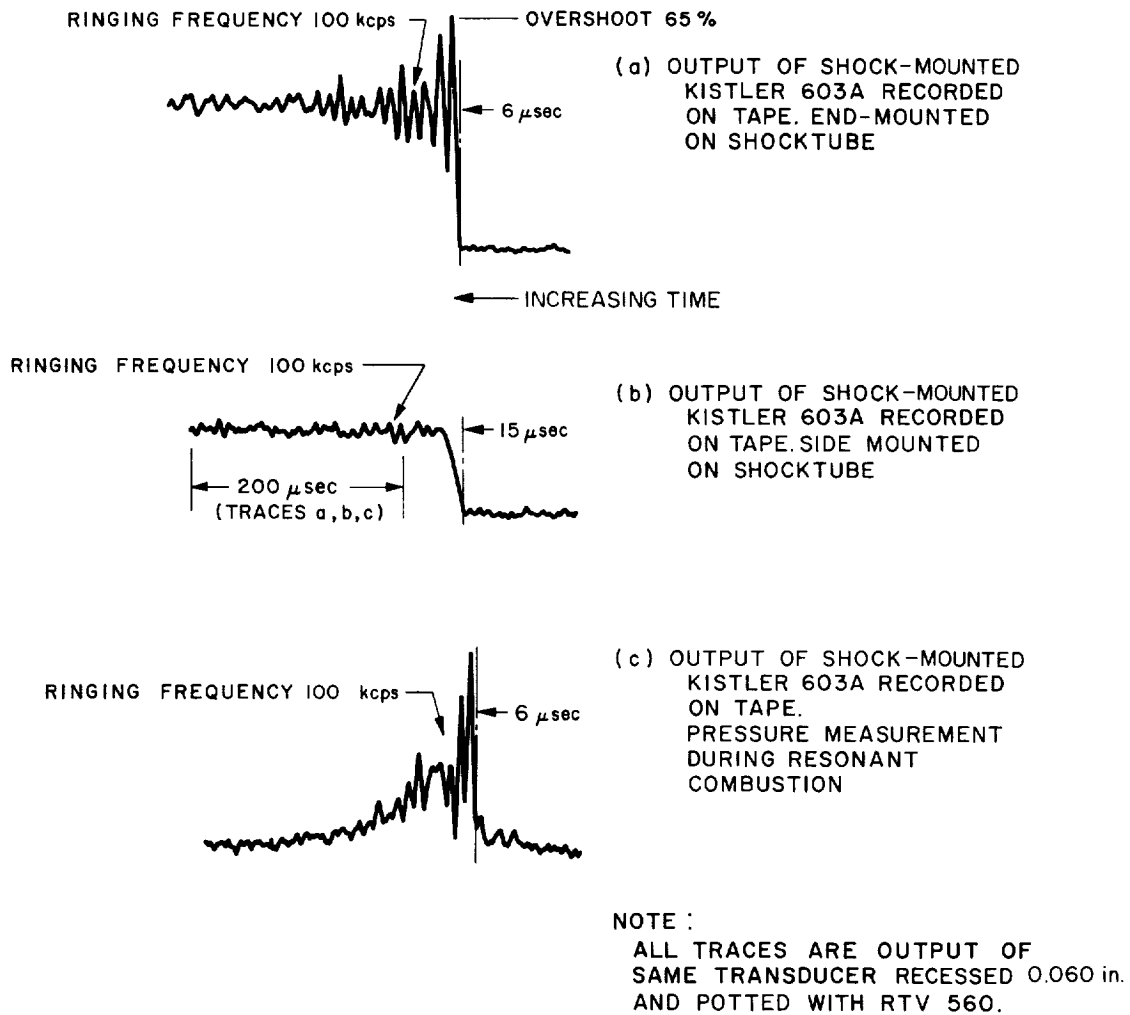


Fig. 18. Comparison of transducer outputs: shock tube tests and resonant combustion

wave on the transducer diaphragm results in a pressure transient with a rise time of the order of 1 μ sec. The significant characteristics of the measurement system response are: (1) rise time of 6 μ sec, (2) overshoot of 65%, and (3) ringing frequency of 100 kcps. Trace (b) is the result of mounting the transducer assembly on the side of the shock tube and exposing it to a shock wave whose transit time across the diaphragm was of the order of 15 μ sec. Note that the recorded rise time coincides with this travel time and that the amount of overshoot is reduced substantially. Trace (c) shows the output of this same transducer during an actual firing.

If one considers the test results of the end-mounted shock tube to be representative of the instrumentation characteristics during resonant combustion conditions, the recorded resonant pressure may be as much as 65% greater than the actual pressure. On the other hand, if

the tests of the side-mounted shock tube are representative of the engine conditions, very little recording overshoot is present. Thus, the amplitude data plotted in Fig. 15 probably has error limits ranging from essentially zero to 65%, depending upon which measurement location is considered. In particular, transducer ringing and hence signal overshoot (albeit of unknown magnitude) was probably encountered along the steeper-fronted areas of the disturbance near the corner of the chamber.

B. Interpretation of Results

With these restrictions in mind concerning the validity of the amplitude data and with a realization that regardless of their accuracy the results do not present the complete spatial description of the resonant disturbance, it nevertheless seems pertinent to assess preliminarily the

hypothesized rotating detonation-like wave concept on the basis of these initial results.

That a high-amplitude, steep-fronted pressure disturbance is rotating about the chamber circumference in a sustained manner seems certain. That the front is a true pressure discontinuity (or shock wave) may not have been rigorously proved owing to the dynamic response limitations of the measurement system. Until this point is resolved, however, by refined experimental techniques (schlieren photography, for instance), it must be concluded that these data do not deny the presence of a shock front and, in fact, strongly imply this probability.

A few details of the spatial orientation of the disturbance front begin to emerge, especially at locations near the injector where the wave intersection with the face and wall seems to have a peculiar shape (Fig. 14). If it is assumed that the extrapolation of the measured intersections to the very corner of the chamber is qualitatively correct, then the following interpretation seems realistic.

The distinct curvature of the intersection in the proximity of the injector-face-to-chamber-wall junction suggests a highly skewed front orientation with this corner. Since the maximum coupling with chemical energy release surely occurs in a chamber prereaction zone where appreciable propellant mixing has been achieved, the highly coupled portion of this skewed front must lie somewhat downstream of the impingement point plane (i.e., $l/L > 0.096$ on Fig. 14). Moreover, if the maximum coupling is somehow attained at a distance inward from the chamber wall (as is suggested by the bulge in the face intersection at $0.6 < r/R < 1.0$ on Fig. 14), then the skewed orientation may be pictured as essentially a rotating "ball of fire" which is continuously driven into and along the corner, becoming squeezed between the highly constraining boundary surfaces in the process.

The fact that the disturbance becomes much less steep-fronted in the inner half-radius of the face seems to locate the driven front in the outer half-radius of the combustion volume. Interestingly enough, the axial dimension of the driven front does not appear to be so clearly indicated—as judged by the smooth wall-intersection curve (downstream of the corner area) and the approximately constant pressure ratio of 10:1 over the range of $0.2 < l/L < 0.5$.

It is believed that this skewed front orientation with the corner explains the very-high-pressure amplitudes

which are observed as these surfaces are approached (Fig. 15), if one considers the increased contribution to the boundary surface pressure due to stagnating the component of gas velocity (immediately behind the front) which is normal to these surfaces. Furthermore, the existence of the very-high-boundary heat flux observed near this corner under resonant conditions (Ref. 2) is believed to be related to the presence of these highly stagnated pressure (hence temperature) conditions. It is interesting to note that the chamber wall areas of this engine which experience the greatest damage during prolonged exposure to resonant combustion extend from the injector end of the chamber to an axial distance of 1 to 1½ in. downstream. An example of this damage is shown in Fig. 19, where severe erosion (giving an undercut appearance) is apparent. The heavily damaged area corresponds to $0.0 < l/L < 0.1$ on Figs. 14 and 15.

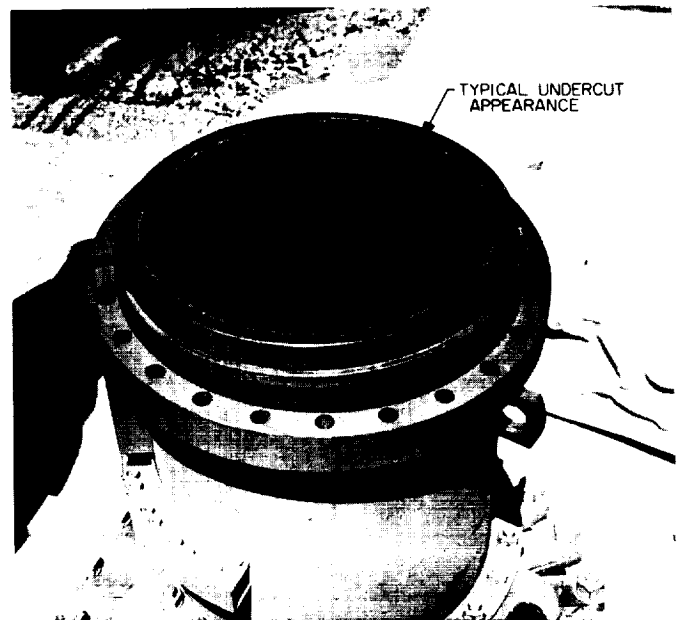


Fig. 19. Chamber wall damage after prolonged exposure to resonant combustion

While the disturbance-to-wall intersection velocity is supersonic ($M = 1.76$ based on an assumed sonic velocity of the chamber gases), the relationship of this intersection Mach number with the actual front propagation velocity (relative to the medium into which the front propagates) is obscure. The deduction of the propagation velocity from boundary measurements must take into account not only the front orientation but also the direction of the gas flow (both with respect to the boundary) when neither of these is yet well defined.

In this sense, the skewed front orientation in the vicinity of the chamber corner implies both radial and axial (in addition to tangential) velocity components relative to the chamber wall which may be associated with the chamber gas flow pattern in this part of the combustion volume. A cursory examination of the time-average pressure distribution across the injector radius has indicated that a pressure gradient exists with decreasing pressure towards the central area; consequently, a radial gas flow into the central volume of the chamber may exist. The general orientation of the face intersection (Fig. 14) seems to indicate that the pressure disturbance is oriented to travel against this radial gas motion. The curvature of the wall intersection (downstream of the corner area) in the direction of wave travel is believed to result from a similar interaction of the disturbance motion on the axial chamber gas flow.

Although further discussion of the nature of the mean gas flow through the chamber and the orientation of the disturbance front does not appear to be warranted on the basis of the experimental results presented herein, it

is concluded that the driven front propagation velocity may be in excess of the 6160 ft/sec intersection velocity.

A few comments on the substantial variations in pressure amplitude which were observed (Fig. 15) are believed to be appropriate. Undoubtedly some of these variations are due to instrumentation dynamic characteristics; yet it is felt that a large part of the amplitude variations must result from local time variant combustion conditions in the medium into which the disturbance propagates. It is noted that the pressure measurements were made over very localized dimensions (transducer diameter = 0.2 in.) on a disturbance which contained a front of very localized nature. The high magnitude of the pressures associated with the pressure wave and the high velocity of the gases following the passage of the wave probably interact to some degree with the injection and subsequent mixing of the propellants. The fact that the observed pressure variations were greatest near the injector supports this viewpoint if it is considered that the result of local combustion variations would tend to be smeared and diminished at downstream locations by the highly turbulent flow conditions in the chamber.

VI. SUMMARY OF RESULTS

The chamber boundary pressure distribution associated with the fully developed rotating mode of resonant combustion exhibited by this engine is characterized by:

1. A disturbance-to-chamber-wall intersection which extends along the entire length of the chamber and has a curvature in the direction of pressure wave rotation such that the nozzle end of the intersection leads the injector end in excess of 40 deg circumferentially.
2. A disturbance-to-injector-face intersection which lies nonradially from the outermost chamber radius into the central area but with a curved shape such that the innermost end of the intersection leads the outermost end substantially.
3. A marked increase in the slope of the intersection curves on both the face and wall surfaces as the junction of these boundaries (i.e., the corner of the chamber) is approached.
4. A varying pressure ratio across the disturbance front (ratio of peak to minimum pressures during a rotation period) which has a maximum observed value exceeding 20:1 very near the corner of the chamber but which decreases to approximately 4:1 near both the nozzle end of the chamber and the central area of the injector face.
5. A disturbance front rise time (from minimum to peak pressure) of less than 3 μ sec in the driven areas of the front near the injector.

While these results were not intended to fulfill an ultimate objective of determining the general applicability of the hypothesized rotating detonation-like wave concept, they are consistent with that thesis. In fact, they provide considerable evidence that for this engine the driven disturbance is shock-fronted and oriented askew with the engine corner surfaces so as to be continuously driven into and along these surfaces in its rotative path of motion.

It is felt that the definition of the parameters controlling rotating resonant combustion, regardless of whether

it is called a detonation or an acoustical disturbance, will require an understanding of the generating and sustaining mechanisms of steep-fronted pressure waves in circular cross-section chambers.

Continued development of high-response diagnostic techniques is required to overcome thermal and mechanical vibration effects and to provide methods of probing the internal combustion volume. The transient response characteristics of these techniques must provide a time resolution of less than 1 μ sec if the local state properties of the resonant disturbance are to be resolved.

NOMENCLATURE

Symbols

A	area, in. ²
C_F	thrust coefficient
C_d	discharge coefficient
F	thrust, lbf
l	axial chamber wall position, in.
L	chamber length, 16.445 in.
L^*	characteristic length, chamber volume/nozzle throat area, in.
M	Mach number
p	pressure, lbf/in. ²
\bar{p}	average pressure value, lbf/in. ²
r	radial position on injector face, in.
R	injector face radius, 5.52 in.
RMS	root mean square

β	complement of true angle between resultant momentum line of injector element and plane normal to chamber axis, deg
γ	ratio of specific heats
ϵ_c	chamber contraction area ratio
ϵ_n	nozzle expansion area ratio
λ	nozzle divergence loss factor

Subscripts

a	atmospheric
c	chamber
e	expansion
exp	expected
f	fuel
min	minimum
ox	oxidizer
pk	peak
t	nozzle throat

REFERENCES

1. Rupe, J. H., *An Experimental Correlation of the Nonreactive Properties of Injection Schemes and Combustion Effects in a Liquid-Propellant Rocket Engine. Part V: On the Influence of Vanes on Combustion and Combustion Stability*, Jet Propulsion Laboratory, Pasadena, California (to be published).
2. Rupe, J. H., and Jaivin, G. I., *The Effects of Injection Mass Flux Distributions and Resonant Combustion on Local Heat Transfer in a Liquid Propellant Rocket Engine*, Technical Report No. 32-648, Jet Propulsion Laboratory, Pasadena, California, October 1, 1964.
3. Krieg, H. C., Jr., "Tangential Mode of Combustion Instability, Detonation and Two-Phase Flow," *Progress in Astronautics and Rocketry*, Vol. 6, Academic Press, 1962.
4. Nicholls, J. A., and Cullen, R.E., "Gaseous Detonation Studies in an Annular Rocket Motor Chamber," *Proceedings of the 1st ICRPG Combustion Instability Conference*, CPIA Publication No. 68, Vol I, pp. 165-184, January 1965.
5. Oppenheim, A. K., and Laderman, A. J., "Role of Detonation in Combustion Instability," *Proceedings of the 1st ICRPG Combustion Instability Conference*, CPIA Publication No. 68, Vol. I, pp. 275-297, January 1965.
6. Denisov, Yj. N., Shchelkin, K. I., and Troshin, Ya. K., "Some Questions of Analogy Between Combustion in a Thrust Chamber and in a Detonation Wave," *Eighth Symposium (International) on Combustion*, pp. 1152-1159, The Williams and Wilkins Co., Baltimore, 1962.
7. Smith, R. P., and Sprenger, D. F., "Combustion Instability in Solid-Propellant Rockets," *4th Symposium on Combustion*, The Williams and Wilkins Co., Baltimore, 1953.
8. Rupe, J. H., *A Correlation Between the Dynamic Properties of a Pair of Impinging Streams and the Uniformity of Mixture Ratio Distribution in the Resulting Spray*, Progress Report No. 20-209, Jet Propulsion Laboratory, Pasadena, California, March 28, 1956.
9. Rupe, J. H., *An Experimental Correlation of the Nonreactive Properties of Injection Schemes and Combustion Effects in a Liquid-Propellant Rocket Engine. Part I: The Application of Nonreactive Spray Properties to Rocket Motor Injector Design*, Technical Report No. 32-684, Jet Propulsion Laboratory, Pasadena, California (to be published).
10. Clayton, R. M., Rupe, J. H., and Gerbracht, F. G., *An Experimental Correlation of the Nonreactive Properties of Injection Schemes and Combustion Effects in a Liquid-Propellant Rocket Engine. Part II: On Experimental Apparatus and Techniques*, Jet Propulsion Laboratory, Pasadena, California (to be published).

REFERENCES (Cont'd)

11. Rupe, J. H., Jaivin, G. I. and Clayton, R. M., *An Experimental Correlation of the Nonreactive Properties of Injection Schemes and Combustion Effects in a Liquid-Propellant Rocket Engine. Part III: On the Relationship Between Gross Performance Level and Injection Schemes*, Jet Propulsion Laboratory, Pasadena, California (to be published).
12. Rogero, S., *Measurement of the High-Frequency-Pressure Phenomena Associated with Rocket Motors*, Technical Report No. 32-624, Jet Propulsion Laboratory, Pasadena, California, May 11, 1964.
13. Inskip, J., *Dynamic Testing of Pressure Transducers—A Progress Report*, Technical Report No. 32-268, Jet Propulsion Laboratory, Pasadena, California, December 6, 1961.

ACKNOWLEDGMENT

The authors would like to express their appreciation to William D. Griffin for his instrumentation engineering support and to Robert J. McKeon and William A. Zahnle for their technical support throughout these experiments.

